Decay of stationary light pulses in ultracold atoms

Jin-Hui Wu,[1] M. Artoni,[2,3] and G. C. La Rocca[4]
[1]*College of Physics, Jilin University, Changchun 130023, People's Republic of China*
[2]*Department of Physics and Chemistry of Materials, CNR-IDASC Sensor Lab, Brescia University, Via Valotti 9, I-25133 Brescia, Italy*
[3]*European Laboratory for Nonlinear Spectroscopy, Via Nello Carrara 1, I-50019 Firenze, Italy*
[4]*Scuola Normale Superiore and CNISM, Piazza dei Cavalieri 7, I-56126 Pisa, Italy*
(Received 17 October 2009; published 11 March 2010)

We develop a general scheme for studying the optical response of ultracold atoms driven into a regime of standing-wave electromagnetically induced transparency. We rely on full numerical solutions of the Maxwell-Liouville equations without invoking secular and adiabatic approximations and arbitrary initial state assumptions. These approximations and assumptions can conceal, e.g., significant loss and diffusion responsible for the decay of stationary light pulses in cold atomic samples. The complex decay dynamics of a stationary light pulse is here analyzed in terms of higher-order spin and optical coherences that arise from nonlinear interactions of the stationary light pulse with the two counterpropagating components of a standing-wave driving field. Specific results for stationary light pulses in cold ^{87}Rb atoms have been discussed for temperature regimes where the residual Doppler broadening is negligible.

DOI: 10.1103/PhysRevA.81.033822 PACS number(s): 42.50.Gy, 42.70.Qs

I. INTRODUCTION

Light waves are quite robust carriers of information while atoms are amenable to accurate quantum-state manipulations [1,2]. Laser-induced excitation of atomic coherence, in particular, has become a rather powerful tool for manipulating both classical and quantum states of light fields. Storage and retrieval of light fields mediated by spin coherence wave packets in atomic samples, for instance, are now practical laboratory routines [3–7]. These typically rely on electromagnetically induced transparency (EIT) [8,9], a well-known phenomenon referring to the resonant absorption suppression of a probe field through destructive quantum coherence established in an atomic sample by a coupling field.

Landmark experiments on storing (retrieving) classical light pulses into (from) atomic spin coherence [4], strongly motivated by early theoretical considerations [3], adopted a *traveling-wave* (TW) driving configuration where a coupling field is used to control the internal electronic states of an atomic sample. Recently, this EIT-based light manipulation technique has led to the demonstration of storage and retrieval of single photons [5], of photonic entanglement [6], and of squeezed vacuum [7]. The TW driving configuration may also be extended to enhance the Kerr-type nonlinear interaction between light signals by introducing more driving fields and atomic states [10–12], which is essential for both classical and quantum information processing.

Capitalizing on the impressive development in the ability to control light-matter interaction in light storage and retrieval experiments, spatially periodic atomic coherences induced by a *standing-wave* (SW) coupling field [13] have further been implemented through standard or modified EIT schemes. It has been found, e.g., that a well-developed photonic bandgap may open up when a SW coupling is applied [14–17], while a stationary light pulse (SLP) has actually been generated when a perfect SW coupling with equal strength forward (FW) and backward (BW) components is switched on [18–22]. Recent advances in this direction are quite promising [23–30], while the issue of how ground-state dephasing [20] and excited state decay [31] may affect the overall SLP decay behavior has recently attracted some interest.

Driving atomic systems in a SW configuration, however, is not a straightforward extension of the TW configuration, as already discussed in Ref. [25]. In a SW driving configuration, higher-order momentum components of spin and optical coherences are expected to arise due to coherent multiple scattering of the FW and BW propagating components of a probe field off the SW driving field. The description of light pulse propagation or SLP generation in the presence of SW driving fields should then take into the proper account the contribution of these higher-order momentum components. These have been shown to come into play, e.g., in the generation of light entanglement [25] through the splitting of an SLP [25,29]. Higher-order momentum components generated through nonlinear Bragg scattering off the SW driving field can preserve their coherence in cold atoms (or impurities doped solids) [20,25] yet may undergo rather quick dephasings in warm vapors due to the atomic random motion [18,19]. This makes the correct description of phenomena associated with the presence of higher-order spin and optical coherence components rather involved and to depend, in particular, on the temperature of the atomic sample. When dealing with warm atoms, the higher-order coherence components can be neglected altogether and this is commonly done by making a secular approximation [19]. Yet, in principle, higher-order coherence components cannot be neglected for cold atoms [25,29] and hence hampering in such a case the validity of the secular approximation.

In this article we seek to establish a rather general framework within which the propagation of a weak probe pulse in ultracold atoms with SW-induced atomic coherence gratings could be studied. Probe pulse propagation is here described in terms of spatial Fourier components of the spin and optical coherences that are coupled to the appropriate Maxwell-Liouville equations. Our method deals in essence

with numerical solutions of these Maxwell-Liouville equations in the presence of a SW coupling field and does not invoke, e.g., secular and adiabatic approximations and arbitrary initial-state assumptions [19,20]. It is here worth mentioning that elegant analytical approaches are also available [25], from which explicit solutions can be obtained only through further simplifications and assumptions. Section II lays the groundwork model needed to illustrate our general approach, which is then employed in Sec. III to investigate on-demand SLP generation in a sample of ultracold ^{87}Rb atoms. Specific to this section is the issue of the SLP decay, which is here addressed by specifically considering the loss and diffusion experienced by the confined SLP. Our solutions show that appreciable loss and diffusion is associated with the excitation of spin and optical coherences higher-order momentum components. These, in fact, turn out to be responsible for an incipient pulse splitting at the onset of the SW coupling field as well as for an increase in the scattering loss channels due to the multiple Bragg scattering of the probe photons off the SW driving field. Conversely, when the higher-order coherence terms are purposely neglected we find little loss and diffusion recovering results that one would rather anticipate for warm atoms [19]. A somewhat similar yet incorrect quenching of SLP loss and diffusion has also been anticipated to occur in ultracold atoms [20]. There numerical calculations with an initial dark-state-polariton assumption (Cf. Eq. (33) in Ref. [20]) take in fact into account only the zero-order spin coherence, leading to a quite different SLP decay behavior. In Sec. IV, we present our concluding remarks and a brief outlook.

II. THEORETICAL MODEL AND BASIC EQUATIONS

We consider an ensemble of Λ-type three-level atoms comprising an excited state $|3\rangle$ and two lower states $|1\rangle$ and $|2\rangle$. A *probe* field of frequency ω_p and wave vector k_p and a *coupling* field of frequency ω_c and wave vector k_c connect the two lower states to the common excited state, respectively. As shown in Fig. 1 this realizes a typical level configuration for the D_2 line in ^{87}Rb atoms where the hyperfine levels $|5S_{1/2}, F=2\rangle$, $|5S_{1/2}, F=1\rangle$ and $|5P_{3/2}, F=2\rangle$ denote, respectively, the states $|1\rangle$, $|2\rangle$ and $|3\rangle$. The dynamics of atomic populations and coherences for this level configuration can be derived through standard procedures which, in the rotating-wave and electric-dipole approximations, lead to a set of *Liouville* equations for the density matrix elements [32]. When the probe field is very weak one can set $\rho_{11} \simeq 1$ and $\rho_{22} \simeq \rho_{33} \simeq \rho_{32} \simeq 0$. In this case the relevant equations describing the time evolution of spin (ρ_{21}) and optical (ρ_{31}) slowly varying (in time) coherences reduce to

$$\begin{aligned} \partial_t \rho_{21} &= -[\gamma_{21} - i(\Delta_p - \Delta_c)]\rho_{21} + i\Omega_c^* \rho_{31} \\ \partial_t \rho_{31} &= -[\gamma_{31} - i\Delta_p]\rho_{31} + i\Omega_c \rho_{21} + i\Omega_p, \end{aligned} \tag{1}$$

where $\Omega_p = E_p d_{31}/2\hbar$ and $\Omega_c = E_c d_{32}/2\hbar$ are Rabi frequencies of the probe and coupling fields, respectively, γ_{21} and γ_{31} describe dephasing rates of the spin and optical coherences, respectively, while $\Delta_p = \omega_p - \omega_{31}$ and $\Delta_c = \omega_c - \omega_{32}$ are the probe and coupling field detunings from corresponding atomic transitions, respectively.

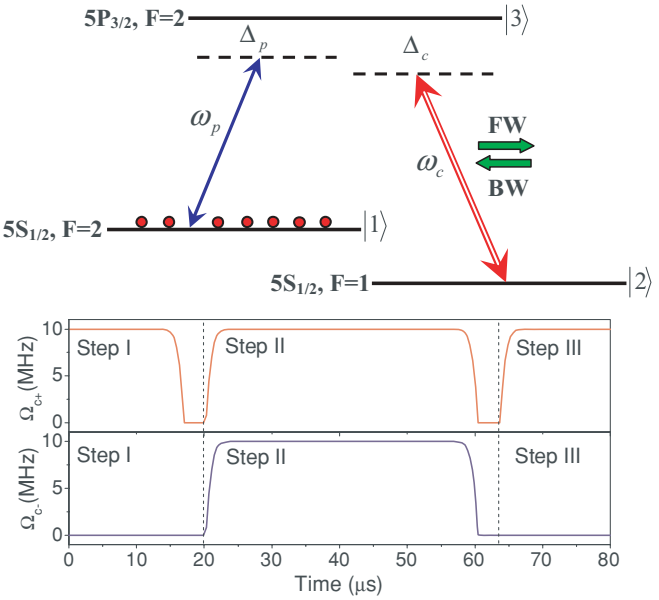

FIG. 1. (Color online) (Upper) Schematic level diagram of an ensemble of ultracold atoms interacting with a weak probe (ω_p) pulse and a strong coupling (ω_c) beam. The levels refer to the D_2 line in ^{87}Rb atoms. (Lower) The FW and BW components of the coupling beam directed along the $+z$ and $-z$ directions, respectively, can be modulated in time so as to achieve "write-in" and "storage" of an incident probe pulse (step I), generation of a "stationary light pulse" (step II), and "read-out" of the probe pulse (step III). The two vertical dotted lines mark off the three different steps.

The coupling field may be either in a TW or in a SW spatial configuration, the latter obtained by the interference of two counterpropagating laser beams. Under suitable conditions a SW driving configuration gives rise to photonic periodic structures where regions of weak and strong normal dispersion periodically alternate with one another [14,16,17]. In the case of a SW coupling field slowly modulated in time, the coupling Rabi frequency in Eqs. (1) takes the form

$$\Omega_c(z,t) = [\Omega_{c+}(t)e^{+ik_c z} + \Omega_{c-}(t)e^{-ik_c z}] \tag{2}$$

where two counterpropagating fields $E_{c+}(t)$ and $E_{c-}(t)$ with Rabi frequencies $\Omega_{c+}(t)$ and $\Omega_{c-}(t)$ are used to control the probe field as shown in Fig. 1. In the presence of such a SW coupling field it is convenient to decompose the probe field into two slowly varying components $E_{p+}(z,t)$ and $E_{p-}(z,t)$ with Rabi frequencies $\Omega_{p+}(z,t)$ and $\Omega_{p-}(z,t)$ so that for $k_p \simeq k_c$ the probe Rabi frequency in Eqs. (1) can be written as

$$\Omega_p(z,t) = [\Omega_{p+}(z,t)e^{+ik_c z} + \Omega_{p-}(z,t)e^{-ik_c z}] \tag{3}$$

The interaction of two coupling fields $E_{c\pm}(z,t)$ with cold atoms in the presence of two probe fields $E_{p\pm}(t)$ gives rise to optical as well as spin coherences with different spatial variations [25,29]. Owing in fact to *multiple* Bragg scattering of FW and BW probe photons off the SW coupling field, distinct coherences will be generated each with its own spatial variation determined by the different momenta acquired through the nonlinear scattering processes (see Fig. 3). The different coherence components are accounted

here by decomposing the spin coherence into Fourier spatial components [19,20]

$$\rho_{21}(z,t)=\sum_{n=-\infty}^{+\infty}\rho_{21}^{(2n)}(z,t)\,e^{+i2nk_cz} \tag{4}$$

and likewise for the optical coherence

$$\rho_{31}(z,t)=\sum_{n=0}^{-\infty}\rho_{31}^{(2n-1)}(z,t)\,e^{+i(2n-1)k_cz}+\sum_{n=0}^{+\infty}\rho_{31}^{(2n+1)}(z,t)\,e^{+i(2n+1)k_cz}, \tag{5}$$

which is purposely written in such a form so as to display its Fourier spatial components of positive and negative orders in a symmetric way. Although the random motion of atoms in warm vapors [18,19] results in a quick dephasing of the higher-momentum components, yet for cold atoms [20,25] these higher-order components do not dephase and affect in principle the dynamics of a light pulse when the atoms are subject to a SW driving as used, e.g., in light storage and retrieval experiments [20,22] and for light entanglement generation [25]. These terms affect to an even greater extent the dynamics of a light pulse in a SW optical grating in impurities doped solids [25,33].

When Eqs. (2)– (5) are inserted into the Liouville Eqs. (1) we attain an infinite set of mutually coupled equations for the spin and optical coherences Fourier components, which are in turn to be coupled to the Maxwell wave equation [17]. In the (space and time) slowly varying envelope approximation, setting $\Delta_p=\Delta_c=0$ for simplicity, we finally arrive at the following coupled Maxwell-Liouville equations

$$\begin{aligned}
\partial_t\rho_{21}^{(2n)}&=-\gamma_{21}\rho_{21}^{(2n)}+i\Omega_{c+}^{*}\rho_{31}^{(2n+1)}+i\Omega_{c-}^{*}\rho_{31}^{(2n-1)},\\
\partial_t\rho_{31}^{(2n\pm1)}&=-\gamma_{31}\rho_{31}^{(2n\pm1)}+i\Omega_{c+}\rho_{21}^{(2n-1\pm1)}\\
&\quad+i\Omega_{c-}\rho_{21}^{(2n+1\pm1)}+i\Omega_{p\pm}\delta_{n,0},\\
\partial_z\Omega_{p+}&=-\partial_t\Omega_{p+}/c+i\Delta k\Omega_{p+}+i\gamma_{31}\alpha\rho_{31}^{(+1)}/2,\\
\partial_z\Omega_{p-}&=+\partial_t\Omega_{p-}/c-i\Delta k\Omega_{p-}-i\gamma_{31}\alpha\rho_{31}^{(-1)}/2,
\end{aligned} \tag{6}$$

with $\alpha=\frac{N_0|d_{31}|^2}{\varepsilon_0\hbar}\frac{k_p}{\gamma_{31}}$ and $\Delta k=k_p-k_c$ and where the space and time dependence of all quantities has no longer been indicated.

In the case where the SW coupling reduces to the TW coupling, the Maxwell-Liouville equations for a FW probe pulse reduce to

$$\begin{aligned}
\partial_t\rho_{21}^{(0)}&=-\gamma_{21}\rho_{21}^{(0)}+i\Omega_{c+}^{*}\rho_{31}^{(+1)},\\
\partial_t\rho_{31}^{(+1)}&=-\gamma_{31}\rho_{31}^{(+1)}+i\Omega_{c+}\rho_{21}^{(0)}+i\Omega_{p+},\\
\partial_z\Omega_{p+}&=-\partial_t\Omega_{p+}/c+i\Delta k\Omega_{p+}+i\gamma_{31}\alpha\rho_{31}^{(+1)}/2,
\end{aligned} \tag{7}$$

for a FW propagating coupling beam, or

$$\begin{aligned}
\partial_t\rho_{21}^{(+2)}&=-\gamma_{21}\rho_{21}^{(+2)}+i\Omega_{c-}^{*}\rho_{31}^{(+1)},\\
\partial_t\rho_{31}^{(+1)}&=-\gamma_{31}\rho_{31}^{(+1)}+i\Omega_{c-}\rho_{21}^{(+2)}+i\Omega_{p+},\\
\partial_z\Omega_{p+}&=-\partial_t\Omega_{p+}/c+i\Delta k\Omega_{p+}+i\gamma_{31}\alpha\rho_{31}^{(+1)}/2,
\end{aligned} \tag{8}$$

for a BW propagating coupling beam. The wave vector mismatch Δk is very small for the D_2 line in ^{87}Rb atoms and may even be made to vanish by slightly misaligning the two counterpropagating FW and BW beams along the z direction [34]. This is indeed the case for all numerical calculations carried out in the next section.

The infinite set of coupled Maxwell-Liouville Eqs. (6) for a SW coupling, whose solutions are obtained through truncations at some cutoff values of $|n|$, along with their counterparts Eqs. (7) and (8), respectively, for an FW coupling and a BW coupling, are our working equations [35]. These will be used in the next section to attain full solutions for the propagation dynamics of a probe pulse in a sample of ultracold ^{87}Rb atoms dressed by a SW coupling. When all coherence components oscillating as $e^{\pm imk_cz}$ with $m>1$ are neglected (i.e., to truncate Eqs. (6) at $|n|=0$), one obtains

$$\begin{aligned}
\partial_t\rho_{21}^{(0)}&=-\gamma_{21}\rho_{21}^{(0)}+i\Omega_{c+}^{*}\rho_{31}^{(+1)}+i\Omega_{c-}^{*}\rho_{31}^{(-1)},\\
\partial_t\rho_{31}^{(\pm1)}&=-\gamma_{31}\rho_{31}^{(\pm1)}+i\Omega_{c\pm}\rho_{21}^{(0)}+i\Omega_{p\pm},\\
\partial_z\Omega_{p\pm}&=\mp\partial_t\Omega_{p\pm}/c\pm i\Delta k\Omega_{p\pm}\pm i\gamma_{31}\alpha\rho_{31}^{(\pm1)}/2,
\end{aligned} \tag{9}$$

which exactly recovers Eqs. (9), (10), and (13) in Ref. [19]. This amounts to the familiar secular approximation used, e.g., to describe the pulse propagation dynamics in a warm atomic vapor. When, on the other hand, all coherence components oscillating as $e^{\pm imk_cz}$ with $m>2$ are neglected, one obtains instead

$$\begin{aligned}
\partial_t\rho_{21}^{(0)}&=-\gamma_{21}\rho_{21}^{(0)}+i\Omega_{c+}^{*}\rho_{31}^{(+1)}+i\Omega_{c-}^{*}\rho_{31}^{(-1)},\\
\partial_t\rho_{31}^{(+1)}&=-\gamma_{31}\rho_{31}^{(+1)}+i\Omega_{c+}\rho_{21}^{(0)}+i\Omega_{c-}\rho_{21}^{(+2)}+i\Omega_{p+},\\
\partial_t\rho_{31}^{(-1)}&=-\gamma_{31}\rho_{31}^{(-1)}+i\Omega_{c+}\rho_{21}^{(-2)}+i\Omega_{c-}\rho_{21}^{(0)}+i\Omega_{p-},\\
\partial_t\rho_{21}^{(+2)}&=-\gamma_{21}\rho_{21}^{(+2)}+i\Omega_{c-}^{*}\rho_{31}^{(+1)},\\
\partial_t\rho_{21}^{(-2)}&=-\gamma_{21}\rho_{21}^{(-2)}+i\Omega_{c+}^{*}\rho_{31}^{(-1)},\\
\partial_z\Omega_{p+}&=-\partial_t\Omega_{p+}/c+i\Delta k\Omega_{p+}+i\gamma_{31}\alpha\rho_{31}^{(+1)}/2,\\
\partial_z\Omega_{p-}&=+\partial_t\Omega_{p-}/c-i\Delta k\Omega_{p-}-i\gamma_{31}\alpha\rho_{31}^{(-1)}/2.
\end{aligned} \tag{10}$$

This specific set of equations [36] have recently been used to model the propagation dynamics of a light pulse in cold ^{87}Rb atoms [22] where the residual Doppler broadening is not negligible.

III. STATIONARY LIGHT IN ULTRACOLD ATOMS

In this section, we investigate the propagation dynamics of a probe pulse across a sample of cold atoms subject to the specific time modulation of the two counterpropagating coupling beams as shown in Fig. 1 for an optimal set of experimental parameters. Three different processes are seen to occur, namely storage of the incident pulse, formation of a SLP, and its subsequent release. The three processes correspond in the order to steps I to III in Fig. 1. We start by examining the time evolution of the probe Rabi frequencies $\Omega_{p\pm}$ together with several spin $[\rho_{21}^{(0)},\ \rho_{21}^{(+10)}]$ and optical $[\rho_{31}^{(+1)},\ \rho_{31}^{(+11)}]$ coherences. This is done by solving the Maxwell-Liouville equations suitably truncated at $|n|=40$ and the relevant results are shown in Fig. 2.

In the first step, a FW probe pulse moves slowly in the atomic sample until stored in the zero-order spin coherence $\rho_{21}^{(0)}$ at a time when the TW coupling is adiabatically switched

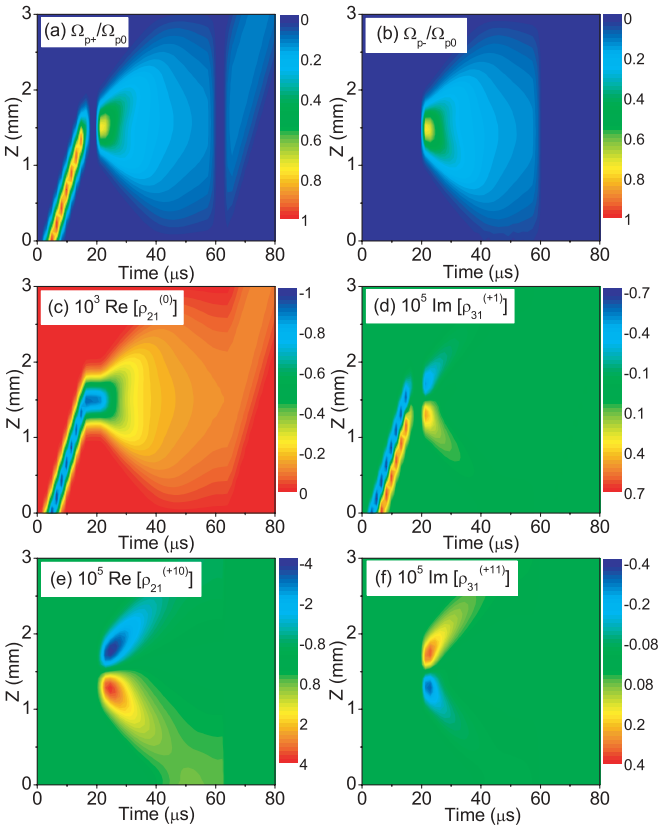

FIG. 2. (Color online) Dynamics of an incident probe pulse moving in the $+z$ direction across a 3-mm-long sample of ultracold ^{87}Rb atoms subject to a time modulation of the FW and BW coupling Rabi frequencies as shown in Fig. 1. All the density plots in (a)–(f) are obtained by truncating Eqs. (6) at $|n| = 40$. Rabi frequencies Ω_{p+} and Ω_{p-} of the two probe components propagating along the $+z$ and $-z$ directions are scaled to the incident probe Rabi frequency Ω_{p0} while $\rho_{21}^{(0)}$, $\rho_{31}^{(+1)}$ and $\rho_{21}^{(+10)}$, $\rho_{31}^{(+11)}$ represent respectively the lowest- and higher-order spin and optical coherence components. The relevant atomic parameters are $\gamma_{21} = 1.0$ kHz, $\gamma_{31} = 6.0$ MHz, $\lambda_p = 780.792$ nm, $\lambda_c = 780.778$ nm, $N_0 = 1.0 \times 10^{13}$ cm^{-3} and $d_{31} = 1.465 \times 10^{-29}$ C m, respectively. The incident probe pulse is assumed to have a Gaussian profile $I_p = I_{p0} \exp[-(t - t_0)^2/\tau^2]$ with $t_0 = 5.0$ μs and duration $\tau = 2.0$ μs. In addition, the probe and coupling detunings are set as $\Delta_p = \Delta_c = 0$ in which case Im$[\rho_{21}]$ and Re$[\rho_{31}]$ are constantly zero [37].

off. Only Ω_{p+}, $\rho_{21}^{(0)}$, and $\rho_{31}^{(+1)}$ are seen to be nonzero, and the maximal amplitude of $\rho_{21}^{(0)}$ is about 0.001 while $\rho_{31}^{(+1)}$ is about two orders of magnitude smaller than $\rho_{21}^{(0)}$. The probe intensity ($\propto \Omega_{p+}^2$), which suffers negligible losses and travels at a very slow velocity, decreases to zero together with the optical coherence $\rho_{31}^{(+1)}$ as the TW coupling is switched off and the FW probe is mapped onto the stationary spin coherence $\rho_{21}^{(0)}$ [3].

In the following step II, when a perfect SW coupling is switched on, both FW and BW probe components are generated from $\rho_{21}^{(0)}$ and somehow frozen in the atomic sample so as to form a SLP, whereas they are mapped back again onto $\rho_{21}^{(0)}$ when the SW coupling is switched off at the end of step II. This SLP is accompanied by the excitation of all spin and optical coherence components having different spatial variations [25,29] in the suitably truncated Maxwell-Liouville Eqs. (6). The leading components $\rho_{21}^{(0)}$ and $\rho_{31}^{(+1)}$ shown in Figs. 2(c) and 2(d) are nonzero [38] as well as the higher-order components such as $\rho_{21}^{(+10)}$ and $\rho_{31}^{(+11)}$ shown in Figs. 2(e) and 2(f). Note, in particular, that the two probe components first quickly increase in amplitude as the SW coupling is switched on and then swiftly decrease in amplitude with an evident spatial spreading after the SW coupling has reached a constant amplitude. This is somewhat at variance with what found, e.g., in Ref. [20] where the two probe components do not decay and diffuse after being generated and it may be here instructive to understand the different decay behaviors.

To this extent we draw our attention to the mutual coupling between spin and optical coherences, as directly inferred from Eqs. (6). This is also schematically shown in Fig. 3 where the zero-order spin coherence $\rho_{21}^{(0)}$, obtained at the end of step I, is set as the source term that gives rise to the probe components $\Omega_{p\pm}$ through the coupling beams $\Omega_{c\pm}$, provided $\rho_{31}^{(\pm1)}$ remain nonvanishing though small in amplitude. For nonvanishing $\rho_{31}^{(\pm1)}$, the actual and only link between the source $\rho_{21}^{(0)}$ and the generated probe components $\Omega_{p\pm}$ during the pulse retrieval at the beginning of step II, all spin and optical coherences in

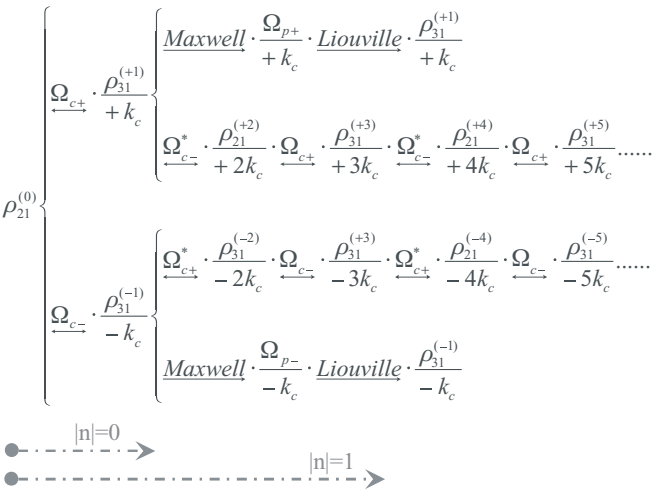

FIG. 3. In ultracold atoms driven by an SW coupling both optical and spin coherences comprise higher-order terms that are excited by their successive interactions with the two counterpropagating components $\Omega_{c\pm}$ of a SW grating (cf. Fig. 1). The diagram illustrates the sequential steps leading to the formation of the first few higher-order spin and optical coherence terms through the mutual interaction between the probe ($\Omega_{p\pm}$) and coupling ($\Omega_{c\pm}$) components, starting from the zero-order spin coherence $\rho_{21}^{(0)}$ generated at the end of step I. The higher the truncation order of the Maxwell-Liouville Eqs. (6) the larger the number of coherence terms that are excited, though the coherence terms gradually decrease in amplitude with their order increasing ($|n| \to \infty$). Equations (6) comprise, e.g., only two coherence terms [$\rho_{21}^{(0)}$, $\rho_{31}^{(\pm1)}$] when truncated at $|n| = 0$, becoming, however, twice as much [$\rho_{21}^{(0)}$, $\rho_{31}^{(\pm1)}$, $\rho_{21}^{(\pm2)}$, $\rho_{31}^{(\pm3)}$] when truncated at $|n| = 1$, as denoted by the two dashed gray lines. The wave vectors associated with different coherence terms are shown right beneath them.

Eqs. (6) will be successively generated from nonlinear Bragg scattering of FW and BW photons according to the pattern illustrated in Fig. 3. As a result of strong coupling ($\Omega_{c\pm} \gtrsim \gamma_{31}$) [39], the first few higher-order optical coherences are typically of the same order of $\rho_{31}^{(\pm 1)}$ [cf. Fig. 2(d) and Fig. 2(f)], while the first few higher-order spin coherences are about 10 times larger than $\rho_{31}^{(\pm 1)}$ [cf. Fig. 2(d) and Fig. 2(e)] mainly because spin coherences are not affected by spontaneous emission. Each excited optical coherence component $\rho_{31}^{(2n\pm 1)}$, dephasing at the rate γ_{31}, works as a scattering loss channel of the source $\rho_{21}^{(0)}$ and the output $\Omega_{p\pm}$ so that we can say a dramatic increase of the scattering loss channels, when Eqs. (6) are truncated at $|n| = 40$, results in the rather quick SLP decay.

In essence, assuming that $\rho_{21}^{(0)}$ is the only nonvanishing (spin) coherence during the SLP formation process may clearly be a source of errors and the reason for departures of our results from those anticipated in Ref. [20]. This may readily be checked by purposely ignoring all higher-order terms [19], which amounts to truncate Eqs. (6) at $|n| = 0$. This is done in Fig. 4, which displays the nonlinear propagation and generation dynamics of $\Omega_{p\pm}$ together with $\rho_{21}^{(0)}$ and $\rho_{31}^{(+1)}$ for the same ultracold atomic sample as in Fig. 2. It is clear that the FW and BW probes experience little loss and diffusion due to the lack of higher-order spin and optical coherences [19,20] when the SW coupling is switched on. One may further see what happens as the cutoff value of $|n|$ is increased. This is shown in Fig. 5 where we compare the dynamic evolution of $\Omega_{p\pm}$, $\rho_{21}^{(0)}$ at $z = 1.5$ mm and $\rho_{31}^{(+1)}$, $\rho_{21}^{(+10)}$, $\rho_{31}^{(+11)}$ at $z = 1.3$ mm for $|n| = 0$, $|n| = 10$, $|n| = 30$, and $|n| = 40$, respectively [40]. We can see that the two probe components and the four coherence components decay faster and faster with increasing $|n|$. Moreover, the difference between the curves for $|n| = 40$ and those for $|n| = 30$ is much smaller than that between the curves for $|n| = 10$ and those for $|n| = 0$. Thus truncating Eqs. (6) at $|n| = 40$ is in this case enough to provide correct

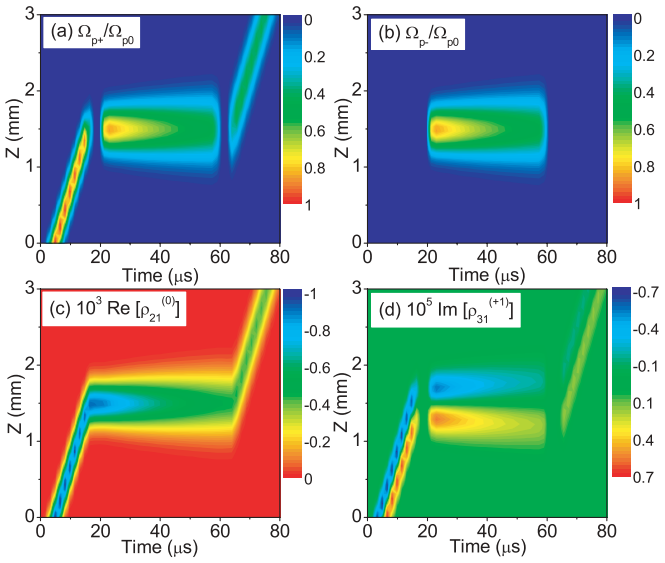

FIG. 4. (Color online) Nonlinear dynamics of an incident probe pulse when all high-order optical and spin coherence components are omitted. The probe and coherence components are the same as in Fig. 2(a)–2(d) yet obtained by truncating Eqs. (6) at $|n| = 0$.

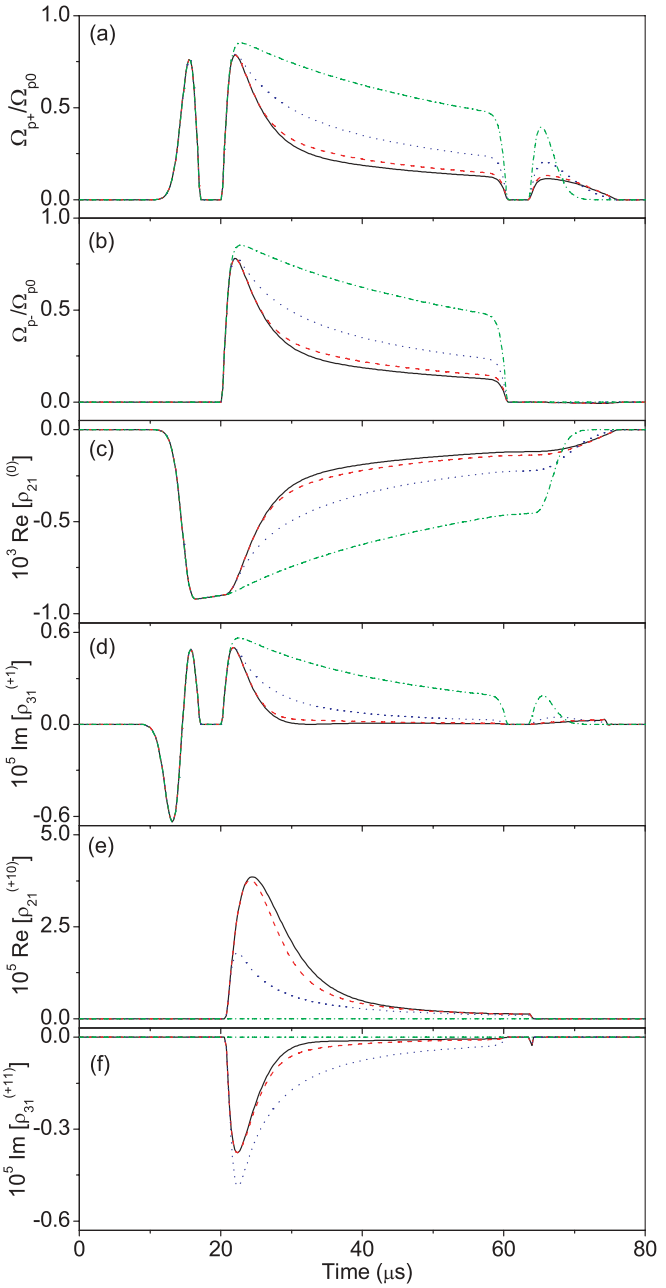

FIG. 5. (Color online) Dynamic evolution of the scaled probe Rabi frequencies $\Omega_{p\pm}$ and spin coherence $\rho_{21}^{(0)}$ evaluated at $z = 1.5$ mm. The other coherence components $\rho_{31}^{(+1)}$, $\rho_{21}^{(+10)}$, and $\rho_{31}^{(+11)}$ are evaluated at $z = 1.3$ mm. The evolution curves are obtained by truncating Eqs. (6) at $|n| = 40$ (black-solid), $|n| = 30$ (red-dashed), $|n| = 10$ (blue-dotted), and $|n| = 0$ (green-dash-dotted), respectively, with the same parameters as in Fig. 2 .

results with a high precision, while lower-order truncations (for instance, at $|n| = 10$ and $|n| = 0$) will result in a severe underestimate of the SLP loss and diffusion.

The appreciable SLP spreading observed in Fig. 2 may be partly attributed to an incipient splitting of the retrieved pulse at the onset of the SW coupling. In other words, the pulse retrieved from $\rho_{21}^{(0)}$ tends to separate into two parts, each containing both Ω_{p+} and Ω_{p-}, moving slowly apart in the FW and BW directions to make their spatial separation in

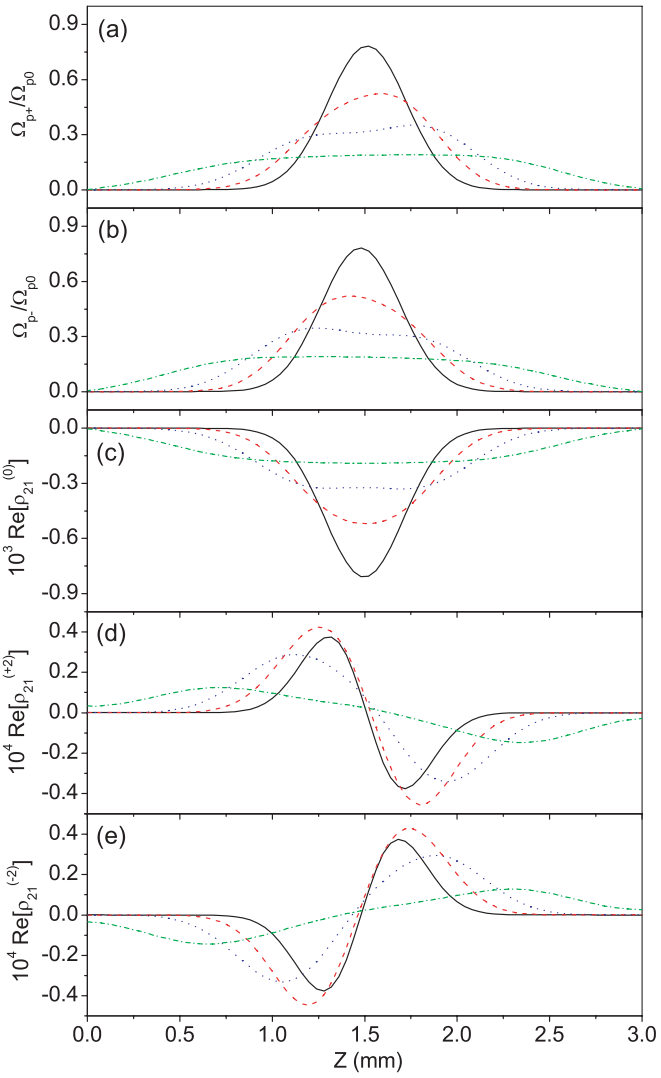

FIG. 6. (Color online) Spatial profiles of the scaled Rabi frequencies $\Omega_{p\pm}$ and the lowest-order spin coherences $\rho_{21}^{(0)}$ and $\rho_{21}^{(\pm 2)}$. The black-solid, red-dashed, blue-dotted, and green-dash-dotted curves correspond to $t = 22.3\ \mu$s, $25.5\ \mu$s, $29.4\ \mu$s, and $39.8\ \mu$s, respectively. All atomic and field parameters are the same as in Fig. 2.

Fig. 2(a) and Fig. 2(b) only slightly perceptible. The SLP trend to separate becomes, however, more apparent at some later stages in the evolution and especially through Fig. 2(d) and Fig. 2(f) where the negative and positive peaks of relevant optical coherence components are seen to move in the opposite directions. We find it instructive to examine the two probe spatial profiles at successive times after retrieval. The spatial profile for Ω_{p+} in Fig. 6(a) , still symmetric for a few μs right after retrieval (black), shows for the subsequent 10 μs interval a clear pull (shift) in the FW direction (red-blue) in spite of the large spreading of the probe component waveform. At times when the spreading becomes larger (green) the two probe components $\Omega_{p\pm}$ become much similar to one another. The FW pulling in Fig. 6(a) (red-blue) is mainly due to the presence of higher-order coherence terms. The space dependence of optical coherence $\rho_{31}^{(+1)}$, which determines in turn the spatial profile of Ω_{p+} through Eqs. (6), originates [41] from small but nonvanishing in-phase (same sign) and out-of-phase (opposite sign) contributions of the asymmetric spin coherence $\rho_{21}^{(+2)}$ added to an otherwise symmetric coherence $\rho_{21}^{(0)}$ [cf. Fig. 6(c) and Fig. 6(d)]. The reverse BW pulling in Fig. 6(b) arises just in the same way [cf. Fig. 6(c) and Fig. 6(e)] and this is what gives rise in the end to the incipient pulse splitting after retrieval. On the other hand, when higher-order terms are neglected, the space dependence of $\rho_{31}^{(+1)}$ is determined only by $\rho_{21}^{(0)}$ [41] in Fig. 4(c) which by itself does not give rise to the typical FW and BW separations observed in Fig. 2(d) and hence preventing spreading of the SLP [cf. Fig. 4(a) and Fig. 4(b)]. It is worthwhile noting, in addition, that spreading dominates over losses (assessed here through the decrease in the two probe intensities $\Omega_{p\pm}^2$ at the succeeding time intervals) in the process of decay of the SLP components shown in Fig. 6(a) and Fig. 6(b).

In the last step III, the FW and BW probes are retrieved in an asymmetric way by switching on a FW coupling to destroy the atomic grating. It is easy to see that, if we simply set $\Omega_{c-} = 0$, Eqs. (6) will become decoupled in the following way:

$$\begin{aligned}
\partial_t \rho_{21}^{(0)} &= -\gamma_{21}\rho_{21}^{(0)} + i\Omega_{c+}^{*}\rho_{31}^{(+1)},\\
\partial_t \rho_{31}^{(+1)} &= -\gamma_{31}\rho_{31}^{(+1)} + i\Omega_{c+}\rho_{21}^{(0)} + i\Omega_{p+},\\
\partial_z \Omega_{p+} &= -\partial_t \Omega_{p+}/c + i\gamma_{31}\alpha\rho_{31}^{(+1)}/2,
\end{aligned} \tag{11}$$

$$\begin{aligned}
\partial_t \rho_{21}^{(-2)} &= -\gamma_{21}\rho_{21}^{(-2)} + i\Omega_{c+}^{*}\rho_{31}^{(-1)},\\
\partial_t \rho_{31}^{(-1)} &= -\gamma_{31}\rho_{31}^{(-1)} + i\Omega_{c+}\rho_{21}^{(-2)} + i\Omega_{p-},\\
\partial_z \Omega_{p-} &= +\partial_t \Omega_{p-}/c - i\gamma_{31}\alpha\rho_{31}^{(-1)}/2,
\end{aligned} \tag{12}$$

$$\begin{aligned}
\partial_t \rho_{21}^{(+2)} &= -\gamma_{21}\rho_{21}^{(+2)} + i\Omega_{c+}^{*}\rho_{31}^{(+3)},\\
\partial_t \rho_{31}^{(+3)} &= -\gamma_{31}\rho_{31}^{(+3)} + i\Omega_{c+}\rho_{21}^{(+2)},
\end{aligned} \tag{13}$$

$$\begin{aligned}
\partial_t \rho_{21}^{(-4)} &= -\gamma_{21}\rho_{21}^{(-4)} + i\Omega_{c+}^{*}\rho_{31}^{(-3)},\\
\partial_t \rho_{31}^{(-3)} &= -\gamma_{31}\rho_{31}^{(-3)} + i\Omega_{c+}\rho_{21}^{(-4)},
\end{aligned} \tag{14}$$

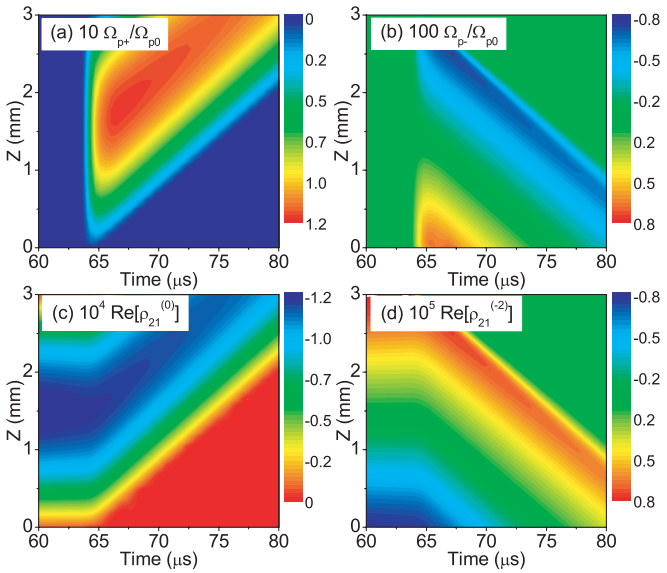

FIG. 7. (Color online) Probe pulse read-out, corresponding to step III in Fig. 2(a) and Fig. 2(b), with two spin coherences $\rho_{21}^{(0)}$ and $\rho_{21}^{(-2)}$ shown below for comparison.

where only the first four sets of equations are listed. For times not much longer than $1/\gamma_{31}$ only $\rho_{21}^{(0)}$ and $\rho_{21}^{(-2)}$, coupled respectively to $\rho_{31}^{(+1)}$ and to $\rho_{31}^{(-1)}$ in the EIT regime, will survive while all other spin coherences will quickly decay to zero. In this case, the pulse dynamics is to a good approximation described only by Eqs. (11) and (12) which describe two decoupled (independent) FW and BW probes. The two probes are different in amplitude and in profile as $\rho_{21}^{(0)}$ and $\rho_{21}^{(-2)}$ do. This is is clearly illustrated in Fig. 7 by blowing up the first three plots in Fig. 2 and adding a new plot for $\rho_{21}^{(-2)}$ during the last 20 μs of the dynamic evolution.

IV. CONCLUSIONS

The dynamics of a reference light pulse passing across a medium exhibiting EIT where the coupling field consists of two counterpropagating components is a fairly involved problem. The complexity arises from the fact that, when a SW grating is formed by two counter-propagating coupling beams of similar wavelengths, nonlinear Bragg scattering of probe photons off the SW grating may excite spatial gratings of higher-order spin and optical coherences [25,29]. The typical framework within which the problem had been studied involves rather drastic secular [19] and adiabatic [19,20] approximations and rather arbitrary initial-state assumptions [20] that are here shown to be not accurate enough at least for ultracold atoms. We take here, in fact, a more general stand on the problems working out solutions of the Maxwell-Liouville equations in the presence of awithout invoking such approximations and assumptions. Our results in Sec. III establish the importance of higher-order coherence components for ultracold atoms and, in particular, their relevance to the issue of the SLP decay, which is here assessed by examining the loss and diffusion experienced by the confined light pulse. Two major effects seem to concur to the loss and diffusion of our probe wavepacket, namely an incipient pulse splitting effect at the onset of the SW driving field and an increase of the scattering loss channels when higher-order optical coherences are excited. Neglecting higher-order optical and spin coherences may not, however, lead to appreciable errors for warm atoms, in which case the higher-order coherence terms quickly decohere due to the fast random atomic motion [19,20].

We expect that our general analysis may prompt a more exhaustive understanding of the SLP dynamics in cold atoms as well as in impurities doped solids [33], which may in turn be exploited to optimize low-loss SLP generation and slow-light pluse confinement [42] for information processing involving all-optically controllable optical gratings.

ACKNOWLEDGMENTS

Jin-Hui Wu gratefully acknowledges the hospitality at Scuola Normale Superiore in Pisa. This work is supported by NSFC-10874057, NCET-06-0309, DYSJ-20070121, and NBRP-2006CB921103 China, the CRUI-British Council Partnership Program on “Atoms and nanostructures”, the IT09L244H5 Azione Integrata grant of M.I.U.R., the PRIN 2006-021037 grant of M.I.U.R., and the CNR contract 0008233 Italy.

[1] L.-M. Duan, M. D. Lukin, J. I. Cirac, and P. Zoller, Nature (London) **414**, 413 (2001).
[2] M. D. Lukin, Rev. Mod. Phys. **75**, 457 (2003).
[3] M. Fleischhauer and M. D. Lukin, Phys. Rev. Lett. **84**, 5094 (2000).
[4] C. Liu, Z. Dutton, C. H. Behroozi, and L. V. Hau, Nature (London) **409**, 490 (2001).
[5] T. Chaneliere, D. N. Matsukevich, S. D. Jenkins, S.-Y. Lan, T. A. B. Kennedy, and A. Kuzmich, Nature (London) **438**, 833 (2005).
[6] K. S. Choi, H. Deng, J. Laurat, and H. J. Kimble, Nature (London) **452**, 67 (2008).
[7] J. Appel, E. Figueroa, D. Korystov, M. Lobino, and A. I. Lvovsky, Phys. Rev. Lett. **100**, 093602 (2008).
[8] S. E. Harris, Phys. Today **50**(7), 36 (1997).
[9] M. Fleischhauer, A. Imamoglu, and J. P. Marangos, Rev. Mod. Phys. **77**, 633 (2005).
[10] C. Ottaviani, D. Vitali, M. Artoni, F. Cataliotti, and P. Tombesi, Phys. Rev. Lett. **90**, 197902 (2003).
[11] Z.-B. Wang, K. P. Marzlin, and B. C. Sanders, Phys. Rev. Lett. **97**, 063901 (2006).
[12] S. Li, X. Yang, X. Cao, C. Zhang, C. Xie, and H. Wang, Phys. Rev. Lett. **101**, 073602 (2008).
[13] For early studies of related atomic coherence effects with SW driving fields see, e.g., F. Silva, J. Mompart, V. Ahufinger, and R. Corbalan, Europhys. Lett. **51**, 286 (2000). See also F. Silva, J. Mompart, V. Ahufinger, and R. Corbalan, in *Modern Challenges in Quantum Optics*, edited by M. Orszag and J. C. Retamal, Lecture Notes in Physics Vol. 575 (Springer, Berlin, 2001), p. 177.
[14] A. Andre and M. D. Lukin, Phys. Rev. Lett. **89**, 143602 (2002).
[15] H. Kang, G. Hernandez, and Y. Zhu, Phys. Rev. Lett. **93**, 073601 (2004).
[16] M. Artoni and G. C. La Rocca, Phys. Rev. Lett. **96**, 073905 (2006).
[17] J.-H. Wu, M. Artoni, and G. C. La Rocca, J. Opt. Soc. Am. B **25**, 1840 (2008).
[18] M. Bajcsy, A. S. Zibrov, and M. D. Lukin, Nature (London) **426**, 638 (2003).
[19] F. E. Zimmer, A. Andre, M. D. Lukin, and M. Fleischhauer, Opt. Commun. **264**, 441 (2006).
[20] K. R. Hansen and K. Mølmer, Phys. Rev. A **75**, 053802 (2007); **75**, 065804 (2007).
[21] F. E. Zimmer, J. Otterbach, R. G. Unanyan, B. W. Shore, and M. Fleischhauer, Phys. Rev. A **77**, 063823 (2008).
[22] Y.-W. Lin, W.-T. Liao, T. Peters, H.-C. Chou, J.-S. Wang, H.-W. Cho, P.-C. Kuan, and I. A. Yu, Phys. Rev. Lett. **102**, 213601 (2009).
[23] A. Andre, M. Bajcsy, A. S. Zibrov, and M. D. Lukin, Phys. Rev. Lett. **94**, 063902 (2005).

[24] A. W. Brown and M. Xiao, Opt. Lett. **30**, 699 (2005).
[25] S. A. Moiseev and B. S. Ham, Phys. Rev. A **71**, 053802 (2005); **73**, 033812 (2006).
[26] B. S. Ham, Appl. Phys. Lett. **88**, 121117 (2006).
[27] D. Petrosyan, Phys. Rev. A **76**, 053823 (2007).
[28] J. Wang, C. Hang, and G. X. Huang, Phys. Lett. A **366**, 528 (2007).
[29] Y. Xue and B. S. Ham, Phys. Rev. A **78**, 053830 (2008).
[30] F. Bariani and I. Carusotto, J. Europ. Opt. Soc. Rap. Public. **3**, 08005 (2008).
[31] G. Nikoghosyan and M. Fleischhauer, Phys. Rev. A **80**, 013818 (2009).
[32] M. O. Scully and M. S. Zubairy, *Quantum Optics* (Cambridge University Press, Cambridge, UK, 1997).
[33] Q.-Y. He, Y. Xue, M. Artoni, G. C. La Rocca, J.-H. Xu, and J.-Y. Gao, Phys. Rev. B **73**, 195124 (2006); J.-H. Wu, G. C. La Rocca, and M. Artoni, *ibid.* **77**, 113106 (2008).
[34] By misaligning the FW and BW components of the SW coupling at an angle χ along z one changes the lattice periodicity $\lambda_c/2 \to \lambda_c/2\cos(\chi/2)$ [16] which amounts to change $k_c \to k_c\cos(\chi/2)$. In Fig. 2, e.g., a small misalignment $\chi = 12$ mrad is sufficient to make $k_c\cos(\chi/2)$ and k_p to be equal.
[35] A stringent check of this numerical Maxwell-Liouville approach has also been carried out through comparison with an exact treatment of the probe propagation based on the transfer-matrix method [17] again confirming the importance of higher-order spin and optical coherences for cold atoms.
[36] Eqs. (10) do not correspond to truncating Eqs. (6) at $|n| = 1$, which would otherwise include two extra equations for the time evolution of optical coherences $\rho_{31}^{(\pm 3)}$.
[37] In the two-photon resonant case ($\Delta_p = \Delta_c = 0$), dynamic equations of $\mathrm{Re}(\rho_{21})$ and $\mathrm{Im}(\rho_{31})$ are decoupled from those of $\mathrm{Im}(\rho_{21})$ and $\mathrm{Re}(\rho_{31})$, which can be easily found from Eqs. (1), so that an incident probe pulse can only excite $\mathrm{Re}(\rho_{21})$ and $\mathrm{Im}(\rho_{31})$ together with the coupling field.
[38] The two leading coherence components exhibit also rather different spatial profiles, a result that is at times disregarded when studying the dynamics of an SLP. Effects of the excited-state decay on the SLP lifetime have been recently studied in Ref. [31] and where in fact the ± 1-order optical coherences in Eq. (8) are taken to have the same spatial profiles as the zero-order spin coherence. In our numerical simulations, instead, no artificial initial boundary conditions are used for the retrieval process in step II.
[39] In the weak coupling limit ($\Omega_{c\pm} \lesssim \gamma_{31}$), though not relevant to the present work, the first few higher-order optical coherences become smaller than $\rho_{31}^{(\pm 1)}$ while the first few higher-order spin coherences are of the same order of $\rho_{31}^{(\pm 1)}$ as numerically checked.
[40] Different spatial positions are adopted to plot the curves shown in Fig. 5 is based on the fact that $\Omega_{p\pm}$ and $\rho_{21}^{(0)}$ have the maximal values at $z = 1.5$ mm while $\rho_{31}^{(+1)}$, $\rho_{21}^{(+10)}$, and $\rho_{31}^{(+11)}$ have the maximal values at $z = 1.3$ mm.
[41] Fig. 6 are plotted at times when $\Omega_{c\pm} \gg \Omega_{p\pm}$ so that the evolution of optical coherence $\rho_{31}^{(+1)}$ in Eqs. (6) is essentially determined by the superposition of the two lowest order terms $\rho_{21}^{(0,+2)}$. When all higher-order terms are neglected as in Fig. 4 only $\rho_{21}^{(0)}$ is instead relevant to the evolution of $\rho_{31}^{(+1)}$ as may directly be inferred from Eqs. (9).
[42] J.-H. Wu, M. Artoni, and G. C. La Rocca, Phys. Rev. Lett. **103**, 133601 (2009).